14th IEA Heat Pump Conference
15-18 May 2023, Chicago, Illinois

Development of dynamic model of variable refrigerant flow cooling system based on moving boundray method

Jeong Kuk Hong, Hongryul Joo, Min Soo Kim*

Department of Mechanical Engineering, Seoul National University, Seoul 08826, Republic of Korea

Abstract

The use of variable refrigerant flow (VRF) cooling and heating systems is gradually expanding, but the development of system dynamic models for optimal operation and fault diagnosis is still in the research stage. Therefore, in this study, we tried to develop a dynamic model of the entire VRF system by modeling the heat exchanger using the moving boundary method. A dynamic model development method for heat exchangers, a receiver, and an accumulator with dynamic variables was presented. In addition, modelling method of shut-down and start-up process in indoor units was also presented. Based on these models, the entire VRF system model was completed by combining static models for components such as compressors. Combining the thermal zone model with the VRF system model, the indoor unit on/off operation of the VRF system was simulated for 2,400 s. The simulation results showed that the developed model simulated the actual VRF system similarly, although there were some errors. However, if the accuracy of the model is increased using actual experimental results in the future, it is expected that the developed model can be used to perform optimal control of the actual VRF system.

Selection and/or peer-review under the responsibility of the organizers of the 14th IEA Heat Pump Conference 2023.

Keywords: Moving boundary method; Variable refrigerant flow; Transient model; Dynamic behavior; Digital twin

1. Introduction

The variable refrigerant flow (VRF) heating and cooling system has higher energy efficiency than duct systems, and it is easy to respond to individual indoor loads, so its market size is continuously increasing [1]. However, the optimal operation method according to changes in indoor load and operating conditions is still in the R&D stage.

Many researchers have struggled to find the optimal operation method of the VRF system. Yun *et al.* [2] developed a load responsive controller for the VRF system which control the evaporating temperature, showing that the new controller could reduce the annual cooling energy consumption by 14%. Moon *et al.* [3] developed two artificial neural network (ANN) model and two control algorithms for finding unoccupied period. Li *et al.* [4] proposed the ANN-based dynamic model for a direct expansion air conditioning system. They showed that the ANN-based model can control appropriately the compressor speed and supply fan speed without other logic.

There are many preceding studies, but in most cases, VRF system models depend on Big Data or utilize VRF system models of commercial programs. However, this method does not guarantee model accuracy for situations where data are not accumulated. Therefore, developing a simulation model that reflects the physical phenomena in the VRF system and using it for optimal control can be a versatile solution.

For this reason, in this study, dynamic model of the entire VRF system by modeling the heat exchanger using the moving boundary method is developed. Also, combining the thermal zone model with the VRF system model, the indoor unit on/off operation of the VRF system is simulated.

* Corresponding author. Tel.: +82-2-880-8362; fax: +82-2-880-4301.
E-mail address: minskim@snu.ac.kr .

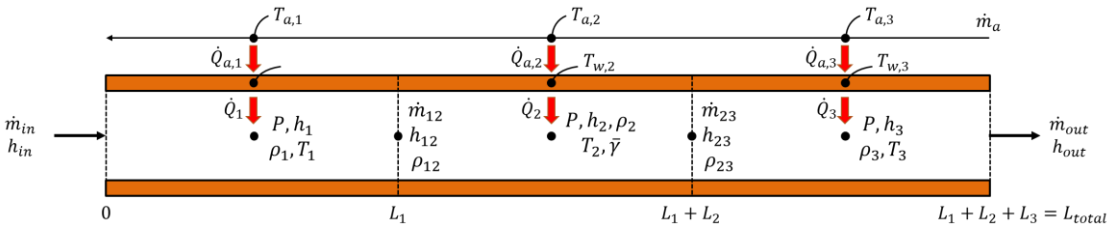

Fig. 1. Illustration of three-zone moving boundary model

2. Model development

2.1. Heat exchanger

2.1.1. Refrigerant mass conservation equations

When modeled by the moving boundary method, the heat exchanger is divided into three regions: subcool, two-phase, and superheat region. In this study, each region was numbered as regions 1, 2, and 3 in order of distance from the heat exchanger inlet. The result of applying the refrigerant mass conservation equation for each region is shown in Eqns. (1)-(3).

$$(\rho_1 - \rho_{12})\dot{L}_1 + \left(\frac{\partial \rho_1}{\partial P}\Big|_{h_1} + \frac{1}{2}\frac{\partial \rho_1}{\partial h_1}\Big|_P \frac{dh_{12}}{dP}\right) L_1 \dot{P} + \frac{1}{2}\frac{\partial \rho_1}{\partial h_1}\Big|_P L_1 \dot{h}_{in} = \frac{\dot{m}_{in} - \dot{m}_{12}}{A} \tag{1}$$

$$(\rho_{12} - \rho_{23})\dot{L}_1 + \left[\bar{\gamma}\rho_g + (1-\bar{\gamma})\rho_f - \rho_{23}\right]\dot{L}_2 + \left[\bar{\gamma}\frac{d\rho_g}{dP} + (1-\bar{\gamma})\frac{d\rho_f}{dP}\right] L_2 \dot{P}$$

$$+ (\rho_g - \rho_f) L_2 \dot{\bar{\gamma}} = \frac{\dot{m}_{12} - \dot{m}_{23}}{A} \tag{2}$$

$$(\rho_{23} - \rho_3)\dot{L}_1 + (\rho_{23} - \rho_3)\dot{L}_2 + \left(\frac{\partial \rho_3}{\partial P}\Big|_{h_3} + \frac{1}{2}\frac{\partial \rho_3}{\partial h_3}\Big|_P \frac{dh_{23}}{dP}\right) L_3 \dot{P} + \frac{1}{2}\frac{\partial \rho_3}{\partial h_3}\Big|_P L_3 \dot{h}_{out} = \frac{\dot{m}_{23} - \dot{m}_{out}}{A} \tag{3}$$

When a certain section disappears within the heat exchanger, the equation derived from that section is no longer applicable. In that case, when section 1 disappears, the equation $\dot{m}_{12} = \dot{m}_{in}$ can be applied instead, and when section 3 disappears, the equation $\dot{m}_{23} = \dot{m}_{in}$ can be applied instead.

2.1.2. Refrigerant energy conservation equations

$$(\rho_1 h_1 - \rho_{12} h_{12})\dot{L}_1 + \left[\left(\frac{\partial \rho_1}{\partial P}\Big|_{h_1} + \frac{1}{2}\frac{\partial \rho_1}{\partial h_1}\Big|_P \frac{dh_{12}}{dP}\right) h_1 + \frac{1}{2}\frac{dh_{12}}{dP}\rho_1 - 1\right] L_1 \dot{P}$$

$$+ \frac{1}{2}\left(h_1 \frac{\partial \rho_1}{\partial h_1}\Big|_P + \rho_1\right) L_1 \dot{h}_{in} = \frac{\dot{m}_{in} h_{in} - \dot{m}_{12} h_{12} + \dot{Q}_1}{A} \tag{4}$$

$$(\rho_{12} h_{12} - \rho_{23} h_{23})\dot{L}_1 + \left[\bar{\gamma}\rho_g h_g + (1-\bar{\gamma})\rho_f h_f - \rho_{23} h_{23}\right]\dot{L}_2$$

$$+ \left[\bar{\gamma}\frac{d\rho_g h_g}{dP} + (1-\bar{\gamma})\frac{d\rho_f h_f}{dP} - 1\right] L_2 \dot{P} + (\rho_g h_g - \rho_f h_f) L_2 \dot{\bar{\gamma}} = \frac{\dot{m}_{12} h_{12} - \dot{m}_{23} h_{23} + \dot{Q}_2}{A} \tag{5}$$

$$(\rho_{23} h_{23} - \rho_3 h_3)\dot{L}_1 + (\rho_{23} h_{23} - \rho_3 h_3)\dot{L}_2 + \left[\left(\frac{\partial \rho_3}{\partial P}\Big|_{h_3} + \frac{1}{2}\frac{\partial \rho_3}{\partial h_3}\Big|_P \frac{dh_{23}}{dP}\right) h_3 + \frac{1}{2}\frac{dh_{23}}{dP}\rho_3 - 1\right] L_3 \dot{P}$$

$$+ \frac{1}{2}\left(h_3 \frac{\partial \rho_3}{\partial h_3}\Big|_P + \rho_3\right) L_3 \dot{h}_{out} = \frac{\dot{m}_{23} h_{23} - \dot{m}_{out} h_{out} + \dot{Q}_3}{A} \tag{6}$$

The result of applying the refrigerant energy conservation equation for each region is shown in Eqns. (4)-(6). When section j disappears, the equation $\dot{L}_j = 0$ can be applied instead of the equation derived from each section.

2.1.3. Tube wall energy conservation equations

$$L_1\dot{T}_{w1} - (T_{w12} - T_{w1})\dot{L}_1 = \frac{\dot{Q}_{a,1} - Q_1}{A_w \rho_w c_w} \tag{7}$$

$$L_2\dot{T}_{w2} + (T_{w12} - T_{w23})\dot{L}_1 - (T_{w23} - T_{w2})\dot{L}_2 = \frac{\dot{Q}_{a,2} - Q_2}{A_w \rho_w c_w} \tag{8}$$

$$L_3\dot{T}_{w3} + (T_{w23} - T_{w3})\dot{L}_1 + (T_{w23} - T_{w3})\dot{L}_2 = \frac{\dot{Q}_{a,3} - Q_3}{A_w \rho_w c_w} \tag{9}$$

The result of applying the tube wall energy conservation equation for each region is shown in Eqns. (7)-(9). The symbol T_{w12} means the tube wall temperature at the boundary between section 1 and section 2, and the T_{w23} means that at the boundary between section 2 and section 3. Some researchers have completed the equation by considering both T_{w12} and T_{w23} to be T_{w2} [5-7]. Also, some researchers have assigned different values to T_{w12} and T_{w23} according to the sign of the time derivative of the length at the boundary point [8-10]. For example, they used T_{w1} for T_{w12} when $\dot{L}_1 < 0$, and they used T_{w2} for T_{w12} when $\dot{L}_1 \geq 0$. However, in this study, Eq. (10) and Eq. (11) were used for expressing T_{w12} and T_{w23} as introduced in [11, 12] because this method is more numerically stable and has no conditional statements.

$$T_{w12} = (L_1 T_2 + L_2 T_1)/(L_1 + L_2) \tag{10}$$

$$T_{w23} = (L_2 T_3 + L_3 T_2)/(L_2 + L_3) \tag{11}$$

2.1.4. Equation for mean void fraction

$$\dot{\bar{\gamma}} = \left(\frac{\partial \bar{\gamma}}{\partial P}\bigg|_{x_{i,2}, x_{o,2}} + \frac{\partial \bar{\gamma}}{\partial x_{i,2}}\bigg|_{P, x_{o,2}} \frac{\partial x_{i,2}}{\partial P}\bigg|_{h_{i,2}} + \frac{\partial \bar{\gamma}}{\partial x_{o,2}}\bigg|_{P, x_{i,2}} \frac{\partial x_{o,2}}{\partial P}\bigg|_{h_{o,2}} \right) \dot{P}$$
$$+ \frac{\partial \bar{\gamma}}{\partial x_{i,2}}\bigg|_{P, x_{o,2}} \frac{\partial x_{i,2}}{\partial h_{i,2}}\bigg|_{P} \dot{h}_{i,2} + \frac{\partial \bar{\gamma}}{\partial x_{o,2}}\bigg|_{P, x_{i,2}} \frac{\partial x_{o,2}}{\partial h_{o,2}}\bigg|_{P} \dot{h}_{o,2} \tag{12}$$

In order to accurately simulate the dynamic behavior of the heat exchanger, the mean void fraction of the two-phase section should be set as a dynamic variable. In this case, one differential equation including quality distribution information within the two-phase section is further required. In this study, Eq. (12) was applied assuming that the refrigerant quality in the two-phase section increases (or decreases) linearly, which was derived in [13, 14]. The subscript $i,2$ means inlet of the two-phase section and the subscript $o,2$ means outlet of the two-phase section

By arranging Eqns. (1)-(12), the dynamic behavior of the heat exchanger is expressed as equations for the vector $[\dot{L}_1, \dot{L}_2, \dot{P}, \dot{h}_{out}, \dot{T}_{w1}, \dot{T}_{w2}, \dot{T}_{w3}, \dot{\bar{\gamma}}]$, and the change in state of the heat exchanger over time can be obtained by integrating this vector.

2.1.5. The situation where the inlet and outlet of the heat exchanger are closed

In a VRF system, some indoor units among several indoor units may stop operating. In this case, generally the fan of the indoor unit still works, but the valves at the inlet and outlet of its heat exchanger are closed and the refrigerant does not flow until the indoor temperature reaches a certain value. In this situation, since the moving boundary method assumes a situation where the refrigerant flows, the governing equations derived in Section 2.1.1 and Section 2.1.2 cannot be applied.

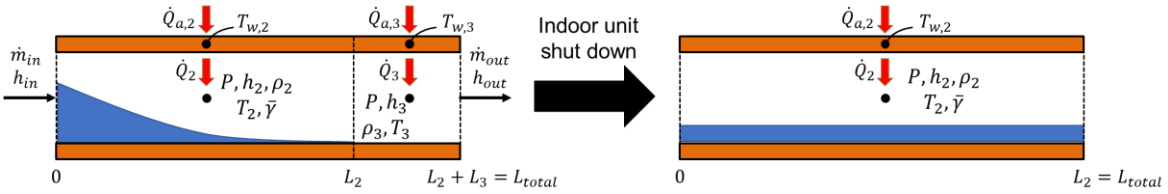

Fig. 2. Change in refrigerant flow inside the heat exchanger when the indoor unit is stopped

$$\left[\bar{\gamma}\frac{d\rho_g}{dP} + (1-\bar{\gamma})\frac{d\rho_f}{dP}\right]\dot{P} + \left(\rho_g - \rho_f\right)\dot{\bar{\gamma}} = 0 \tag{13}$$

$$\left[\bar{\gamma}\left(\rho_g\frac{du_g}{dP} + \frac{d\rho_g}{dP}u_g\right) + (1-\bar{\gamma})\left(\rho_f\frac{du_f}{dP} + \frac{d\rho_f}{dP}u_f\right)\right]\dot{P} + \left(\rho_g u_g - \rho_f u_f\right)\dot{\bar{\gamma}} = \frac{\dot{Q}_2}{AL_2} \tag{14}$$

Therefore, Eq. (13) and Eq. (14) were derived for the situation. Since there is no mass flow of the refrigerant, the mass in the heat exchanger does not change and thus $\dot{\rho}_2 = 0$. Then, since $\rho_2 = \bar{\gamma}\rho_g + (1-\bar{\gamma})\rho_f$, Eq. (13) can be derived. By similar way, from $(m_2 u_2)' = (AL_2\rho_2 u_2)' = \dot{Q}_2$ and $\rho_2 u_2 = \bar{\gamma}\rho_g u_g + (1-\bar{\gamma})\rho_f u_f$, Eq. (14) can be derived.

Since the Eq. (8) still can be used when indoor unit stopped, therefore the dynamic behavior of the heat exchanger is expressed as equations for the vector $[\dot{P}, \dot{T}_{w2}, \dot{\bar{\gamma}}]$.

2.2. Accumulator and receiver

$$\dot{m}_{acc} = \dot{m}_{acc,in} - \dot{m}_{acc,out} \tag{15}$$

$$\frac{d(m_{acc}u_{acc})}{dt} = \dot{m}_{acc}u_{acc} + m_{acc}\dot{u}_{acc} = \dot{m}_{acc,in}h_{acc,in} - \dot{m}_{acc,out}h_{acc,out} \tag{16}$$

$$\dot{u}_{acc} = \frac{\partial u_{acc}}{\partial P}\bigg|_{\rho_{acc}}\dot{P} + \frac{\partial u_{acc}}{\partial \rho_{acc}}\bigg|_{P}\frac{1}{V_{acc}}\dot{m}_{acc} \tag{17}$$

$$m_{acc}\frac{\partial u_{acc}}{\partial P}\bigg|_{\rho_{acc}}\dot{P} + \left(u_{acc} + \frac{\partial u_{acc}}{\partial \rho_{acc}}\rho_{acc}\right)\dot{m}_{acc} = \dot{m}_{acc,in}h_{acc,in} - \dot{m}_{acc,out}h_{acc,out} \tag{18}$$

Since the accumulator and receiver can store the refrigerant mass inside the components, the change in the mass of the refrigerant inside the components is expressed as a dynamic behavior. Taking an accumulator as an example, the change in refrigerant mass in the accumulator is expressed as the difference between the mass flow rate at the inlet and the mass flow rate at the outlet, as shown in Eq. (15). Also, energy balance equation was derived as Eq. (16). By thermodynamics, u_{acc} could be expressed with other two thermodynamic properties such as P and ρ_{acc} and Eq. (17) was derived as a result. Combining Eq. (16) and Eq. (17), finally Eq. (18) was obtained. It is noteworthy that the outlet enthalpy ($h_{acc,out}$) become h_g or h_{acc}, respectively, depending on whether the refrigerant inside the accumulator is in a two-phase state or a single-phase state. As a conclusion, the dynamic behavior of the accumulator and receiver is expressed as equations for the vector $[\dot{P}, \dot{m}_{acc}]$ *or* $[\dot{P}, \dot{m}_{rec}]$.

2.3. Compressor, electronic expansion valve (EEV), and pipe

Since the time constants of a compressor and an EEV are very small compared to that of heat exchangers, a static model is used for the compressor and expansion valve, not a dynamic model. In addition, in the case of a pipe connecting the indoor unit and the outdoor unit, the mass of the refrigerant can be stored therein, but the amount is very small compared to the heat exchanger, the accumulator, and the receiver. Therefore, the static pipe model is also used for pipes.

As a static model for the compressor, refrigerant flow in compressor can be calculated as the product of the compressor frequency, inlet refrigerant density, and stroke volume. The compressor outlet enthalpy can be calculated with an isentropic efficiency. As a static model for the EEV, refrigerant flow in EEV can be

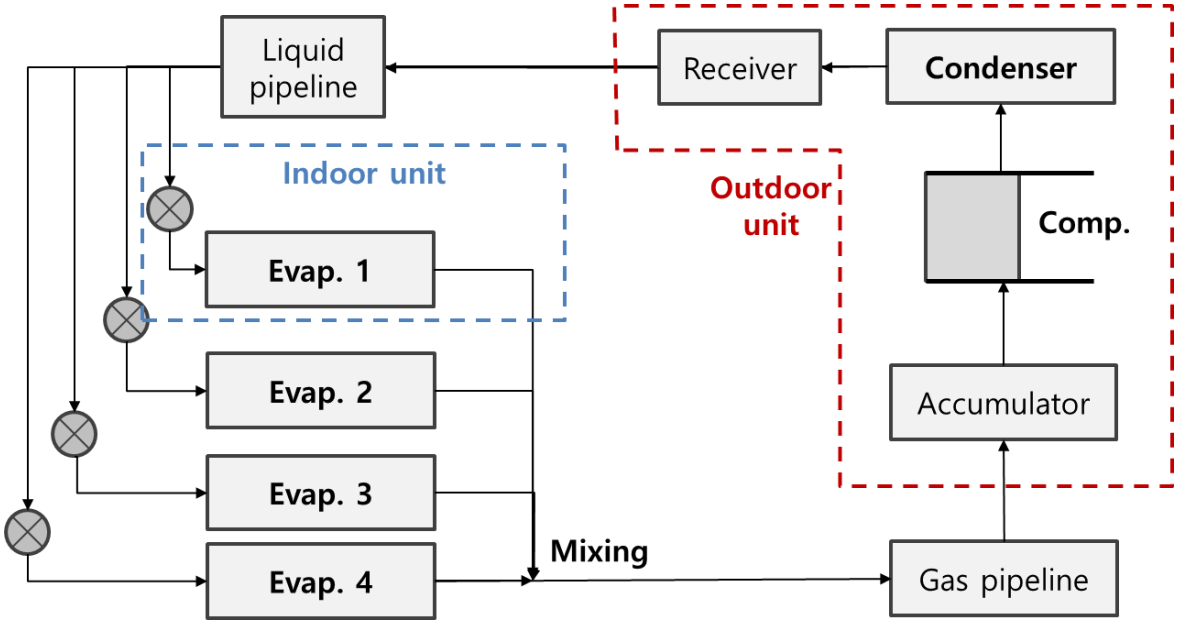

Fig. 3. Schematic diagram of the simulated VRF system

determined by the orifice flow equation, and the outlet enthalpy was the same as the inlet enthalpy. For calculating pressure drop in pipes, Darcy-Weisbach equation was used.

2.4. System configuration

In this study, a dynamic model of a VRF system including one outdoor unit, four indoor units, a compressor, four EEVs, an accumulator, and a receiver was developed as shown in Fig. 3. The simulation was performed only in cooling mode and cooling capacity of the VRF system was set to 30 kW. PI control was applied to the compressor speed so that the accumulator pressure, which is the inlet pressure of the compressor, reached a specific value from the initial condition of 0 Hz. In addition, the openings of the EEVs were also PI controlled so that the superheat at the outlet of each indoor unit be 10 K. In the case of the indoor unit, on/off control was applied, and the refrigerant flow was stopped when the air inlet temperature reached 17.5℃, and the valve was opened to allow the refrigerant to flow when the temperature reached 18.5℃. Other simulation conditions, parameters, and component geometry not mentioned are shown in Table 1.

Table 1. VRF system simulation conditions

Item	Value
Refrigerant	R-410A, Charge = 11.4 [kg]
Indoor/Outdoor T	27, 25, 23, 21 / 35 [℃] at initial
Compressor	$V = 150$ [cc], $\eta_{isen} = 0.75, \eta_v = 1$, Hz = 15 ~ 60 (PID controlled for matching accumulator pressure)
EEV	$\dot{m}_{EEV} = C_V\sqrt{\rho_{in}(P_{in} - P_{out})}$ DSH1 = DSH2 = DSH3 = DSH4 = 10 K (PI controlled)
Condenser	154 × 7.2 × 176 [cm^3] Finned-tube heat exchanger Heat transfer coefficient: single-phase from Gnielinski (1976), two-phase from Chen (1987) Air mass flowrate: 220 [m^3/min]
Evaporator	175 × 4 × 24 [cm^3] Finned-tube heat exchanger Heat transfer coefficient: single-phase from Gnielinski (1976), two-phase from Chen (1966) Air mass flowrate: 19 [m^3/min]
Receiver	*V*=13 [L]
Accumulator	*V*=5.7 [L]

2.5. Thermal zone model

Thermal zone models were constructed to simulate the situation where the indoor temperature decreases due to the cooling operation of the VRF system and the indoor unit repeats on/off. The thermal zone modeling method referred to the study of Lapusan *et al.* [15] Lapusan *et al.* constructed thermal resistance circuit for the multi-room building considering conduction from ceiling, interior and external wall, windows, and floor; ventilation through the windows; radiation from the sun.

By modifying their thermal resistance model, the thermal resistance model to be applied to this simulation was developed as shown in Fig. 4. Cooling effect from the VRF system and heat generation from human beings were added to the previous model.

The size, arrangement, and other simulation conditions of each thermal zone are shown in Fig. 5. The ground temperature was set to 10℃ and the amount of solar radiation and heat generation were set to 160 W and 500 W (5 people in each room), respectively. Additionally, mass flow rate of the ventilation was set to 50 m^3/h. In term of geometry, each room has an area of 25 m^2 and a height of 3 m and all four rooms are placed side by side.

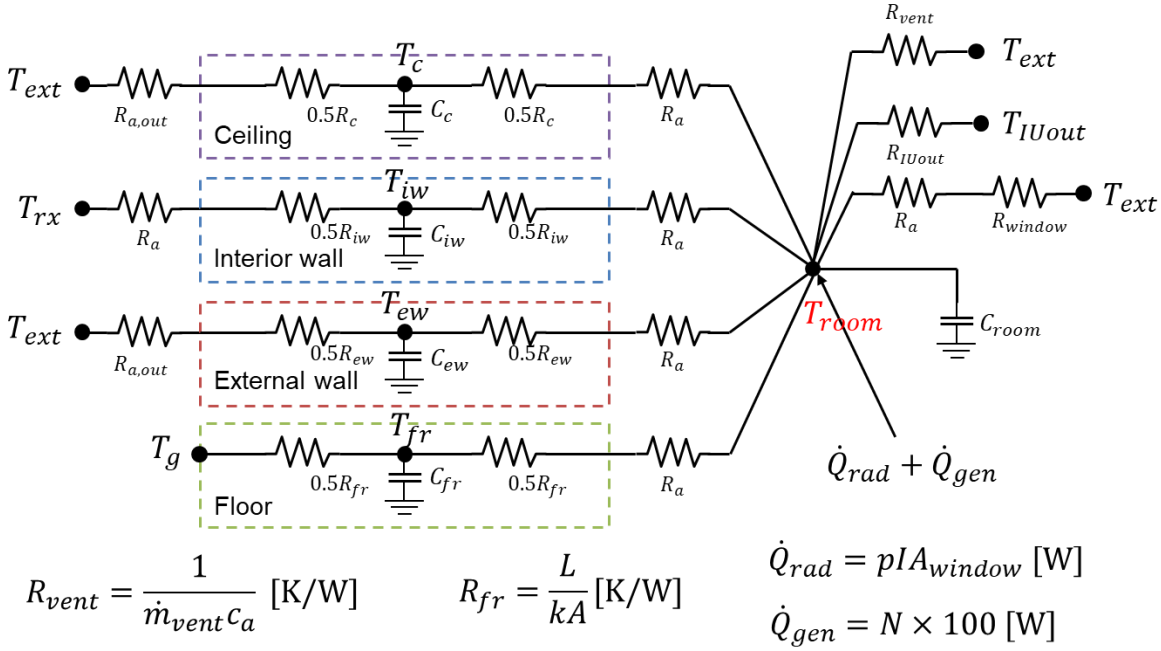

Fig. 4. Thermal resistance circuit for one room in the multi-room building

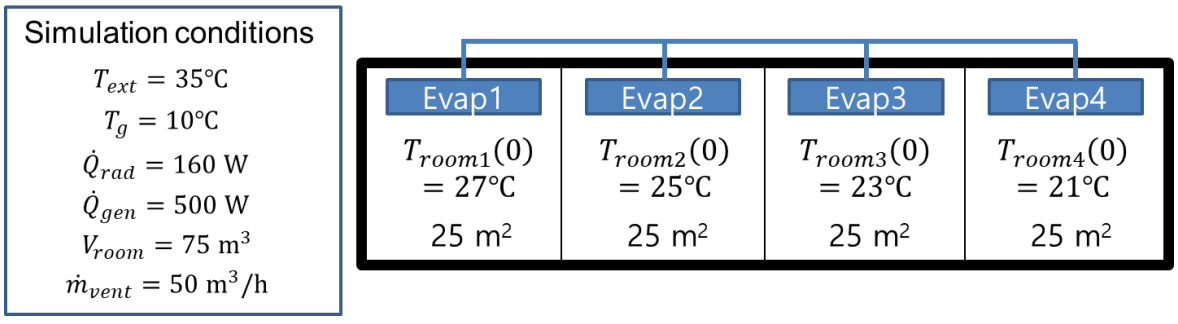

Fig. 5. 4-office zone arrangement for VRF cooling system simulation and simulation conditions

3. Simulation results

Fig. 6 shows the dynamic behaviors of the simulated system from 0 s to 2,400 s. At 690 s, inlet air temperature of the fourth evaporator reached the set lower limit, and the valves of that indoor unit were closed.

Then, the pressure of the refrigerant in the indoor unit rapidly increased as heat was supplied from the indoor air. When the temperature of the refrigerant became the same as the room temperature, the heat transfer decreased and it approached a steady state with no pressure change. Sequentially, the other indoor units also experienced the same process. At 1,350 s, inlet air temperature of the fourth evaporator reached the set upper limit and valves were opened. Then, the refrigerant in the indoor unit quickly moved to the accumulator which had lower pressure, and the indoor unit pressure drastically decreased. Although the slope of decreasing pressure was very large, the simulation was robust and worked without showing numerical instability even when this process was repeated.

However, as the simulation time elapsed, the compressor inlet pressure (accumulator pressure) converged to about 620 kPa. This is the evaporation pressure corresponding to the evaporation temperature of -7.6℃, and it shows a difference from the operating data of the actual VRF system. This difference is expected to be resolved through a model validation process that and reduces the error with the experimental results of the actual VRF system changing the main parameters of the VRF system modeling.

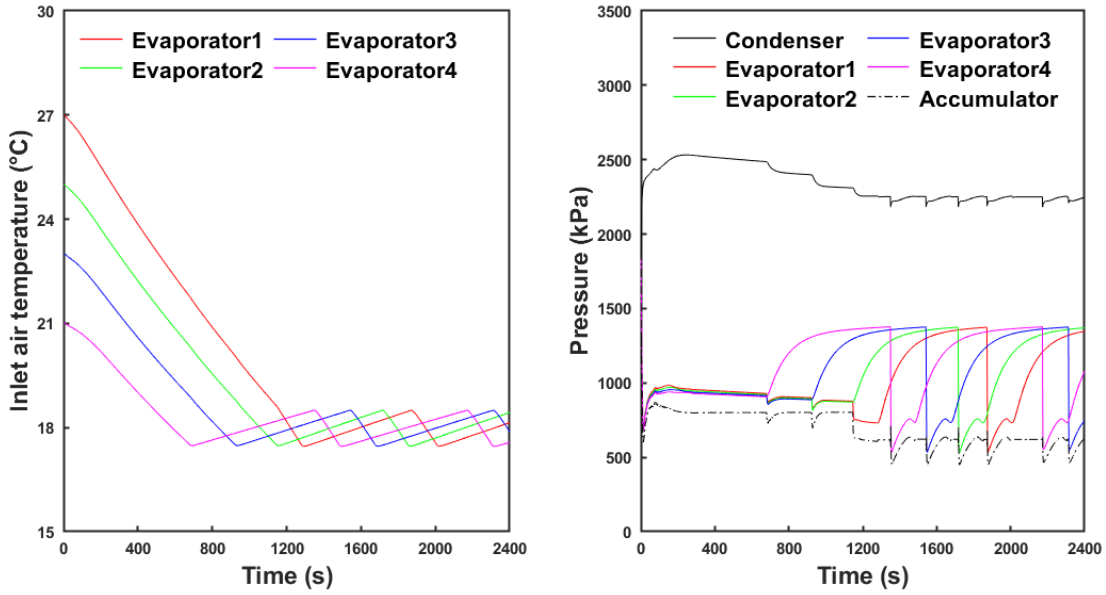

(a) (b)

Fig. 6. Dynamic behaviors of the simulated system (a) Inlet air temperature in each zone (b) Pressure of the components

4. Conclusions

In this study, the heat exchanger was modeled using the moving boundary method, and the dynamic model development and simulation of the entire VRF system was performed by combining it with the main component models of the VRF system. In particular, a modeling method in the stationary state of the indoor unit, which frequently occurs in VRF systems, was included. In addition, the indoor unit on/off operation of the VRF system was simulated by combining the thermal zone model. Based on the system pressure change data derived through simulation, it was confirmed that the developed model simulated the actual VRF system similarly, although there were some errors. However, if the accuracy of the model is increased using actual experimental results in the future, it is expected that the developed model can be used to perform optimal control of the actual VRF system.

Nomenclature

A	=	Cross-sectional area [m^2]
C	=	Heat capacity [J/K]
c	=	Specific heat capacity [J/(kg·K)]
$\bar{\gamma}$	=	Mean void fraction [-]
h	=	Specific enthalpy [J/kg]
η_{isen}	=	Isentropic efficiency [-]
η_v	=	Volumetric efficiency [-]
I	=	Solar radiation = 80 [W/m^2]
k	=	Thermal conductivity [W/(m·K)]
L	=	Length [m]
m	=	Mass [kg]
$\dot{m}$	=	Mass flow rate [kg/s]
N	=	The number of occupants [-]
P	=	Pressure [Pa]
p	=	Fraction of solar radiation transmitted to the floor = 0.6 [-]
$\dot{Q}$	=	Heat transfer rate [W]
R	=	Thermal resistance [K/W]
ρ	=	Density [kg/m^3]
T	=	Temperature [K]
T_{ext}	=	Outdoor temperature [K]
T_g	=	Ground temperature [K]
t	=	Time [s]
u	=	Specific internal energy [J/kg]
V	=	Volume [m^3]
$x_{i,2}$	=	Quality at two-phase section inlet [-]
$x_{o,2}$	=	Quality at two-phase section outlet [-]

Subscript

1	=	Section 1
12	=	Boundary between section 1 and section 2
2	=	Section 2
23	=	Boundary between section 2 and section 3
3	=	Section 3
a	=	Air
acc	=	Accumulator
c	=	Ceiling
ew	=	External wall
f	=	Liquid
fr	=	Floor
g	=	Gas
gen	=	Generation
in	=	Inlet
iw	=	Interial wall
out	=	Outlet
rad	=	Radiation
rec	=	Receiver
$room$	=	Room
rx	=	Adjacent room
$vent$	=	Ventilation

w	=	Tube wall
$window$	=	Window

References

[1] Wan, H., Cao, T., Hwang, Y., Oh, S., 2020. *A review of recent advancements of variable refrigerant flow air-conditioning systems*. Appl. Therm. Eng. 169, 114893.

[2] Yun, G.Y., Lee, J.H., Kim, H.J., 2016. *Development and application of the load responsive control of the evaporating temperature in a VRF system for cooling energy savings*. Energy Build. 116, 638–645.

[3] Moon, J.W., Jung, S.K., 2016. *Development of a thermal control algorithm using artificial neural network models for improved thermal comfort and energy efficiency in accommodation buildings*. Appl. Therm. Eng. 103, 1135–1144.

[4] Li, N., Xia, L., Shiming, D., Xu, X., Chan, M.-Y., 2012. *Dynamic modeling and control of a direct expansion air conditioning system using artificial neural network*. Appl. Energy 91, 290–300.

[5] Willatzen, M., Pettit, N.B.O.L., Ploug-Sørensen, L., 1998. *A general dynamic simulation model for evaporators and condensers in refrigeration. Part I: moving-boundary formulation of two-phase flows with heat exchange: Modèle général dynamique pour évaporateurs et condenseurs frigorifiques. Partic I: Formulation des conditions aux limites variables de flux biphasiques avec échange de chaleur*. Int. J. Refrig. 21, 398–403.

[6] Shah, R., Alleyne, A.G., Bullard, C.W., Rasmussen, B.P., Hrnjak, P.S., 2003. *Dynamic modeling and control of single and multi-evaporator subcritical vapor compression systems.*

[7] Eldredge, B.D., Rasmussen, B.P., Alleyne, A.G., 2008. *Moving-Boundary Heat Exchanger Models With Variable Outlet Phase*. J. Dyn. Syst. Meas. Control 130. https://doi.org/10.1115/1.2977466

[8] Jensen, J.M., Tummescheit, H., 2002. *Moving boundary models for dynamic simulations of two-phase flows*, in: Proc. of the 2nd Int. Modelica Conference.

[9] McKinley, T.L., Alleyne, A.G., 2008. *An advanced nonlinear switched heat exchanger model for vapor compression cycles using the moving-boundary method*. Int. J. Refrig. 31, 1253–1264.

[10] Zapata, J.I., Pye, J., Lovegrove, K., 2013. *A transient model for the heat exchange in a solar thermal once through cavity receiver*. Sol. Energy 93, 280–293.

[11] Zhang, W.J., Zhang, C.L., 2006. *A generalized moving-boundary model for transient simulation of dry-expansion evaporators under larger disturbances*. Int. J. Refrig. 29, 1119–1127.

[12] Bonilla, J., Dormido, S., Cellier, F.E., 2015. *Switching moving boundary models for two-phase flow evaporators and condensers*. Commun. Nonlinear Sci. Numer. Simul. 20, 743–768.

[13] Qiao, H., Aute, V., Radermacher, R., 2014. *An improved moving boundary heat exchanger model with pressure drop*. Int. Refrig. Air Cond. Conf.

[14] Qiao, H., Laughman, C.R., Aute, V., Radermacher, R., 2016. *An advanced switching moving boundary heat exchanger model with pressure drop*. Int. J. Refrig. 65, 154–171.

[15] Lapusan, C., Balan, R., Ciprian, R.A.D., Plesa, A., 2015. *Development of a multi-Room building thermal model for use in the design process of energy management systems*. ACTA Tech. NAPOCENSIS-Series Appl. Math. Mech. Eng. 58.